AMS Home   Journals Home   Journal Archive   Subscribe   For Authors   Help   Advanced Search   Search [Go]

Full Text View

Study of Spatial Spectra of Horizontal Turbulence in the Ocean Using Drifter Data

Im Sang Oh

Department of Oceanography and Research Institute of Oceanography, Seoul National University, Seoul, Korea

Victor Zhurbas

Shirshov Institute of Oceanology, Moscow, Russia

ABSTRACT

The statistics of a pair of Lagrangian particles offer, in principle, a possibility to estimate the structure functions of velocity, then the spatial autocorrelations, and finally the spatial spectra. On the basis of this strategy, the authors have developed an approach to estimate spatial spectra of mesoscale horizontal turbulence in the ocean using data of satellite-tracked drifters. The approach was applied to the data of 19 drifters deployed in the California Current System in 1993. It was found that the shape of both those spectra and this spectra calculated using drifterborne longitudinal and transverse correlations estimated by other authors are qualitatively in good accordance with theoretical predictions for 2D isotropic nondivergent turbulent flow. To relate obtained spectra to some physical parameters, kinematic stochastic models were developed that consisted of a population of randomly spaced, 2D axisymmetric eddies of a given shape. Numerical experiments with different eddy shapes showed that the model spectra obey a self-similarity; that is, at a given eddy shape they depend on the variance of stochastic process and a length scale of the eddy only. A model with the exponential eddy shape was found to fit drifterborne spectra better than other models. The best agreement between the drifterborne and model spectra was achieved when the radius of an exponentially shaped model eddy was taken equal to the internal Rossby radius.

Options:
- Create Reference
- Email this Article
- Add to MyArchive
- Search AMS Glossary

Search CrossRef for:
- Articles Citing This Article

Search Google Scholar for:
- Im Sang Oh
- Victor Zhurbas

1. Introduction

During the last two decades, satellite-tracked drifters have become a powerful tool for observing the general ocean circulation and mesoscale motions at coherent structures like fronts, eddies, and jetlike currents. In particular, the basic transport processes in a flow are most explicitly described in the Lagrangian reference frame so that drifting buoy observations (which are quasi-Lagrangian) are well suited for describing the effects of eddy variability on mean transport (Davis 1991). These processes are most frequently summarized in terms of an eddy diffusivity, which is a parameterization of the effects of small-scale, unresolved motions on the large-scale, resolved flow.

Applications of satellite-tracked drifter data to study transport processes are based on both one-particle statistics (Davis 1987, 1991; Figueroa and Olson 1989; Grifa et al. 1995; Krauss and Boning 1987; Rossby et al. 1983; Swenson and Niiler 1996) and particle-pair statistics (Davis 1985; Poulain and Niiler 1989). There is at least one issue in which the two-particle

statistics, that is, considering relative velocities and displacements of a pair of drifters, seems very attractive and promising. Namely, the particle pair approach offers a possibility to examine statistically the spatial structure of mesoscale ocean eddies, that is, the horizontal turbulence (Middleton and Garrett 1986). This paper is an attempt to determine spectra of horizontal turbulence in the ocean applying the particle pair approach to available satellite-tracked drifter data.

2. Dataset

We obtained the data for this study from a global dataset of ocean surface currents and temperature collected for the WOCE/TOGA Surface Velocity Program (Hansen and Poulain 1996). In accordance with the procedure to be applied, we were looking for an experiment in which as many as possible drifting buoys were deployed simultaneously at about the same position. We selected an experiment in which 19 drifters were deployed in the California Current System on 19 September 1993, at about 37.5°N, 125°W. The drifters were drogued to 15-m depth. All buoy transmitters were programmed to transmit continuously for an initial 90-day period so that there were several observations within a day. In our analysis, we used the data obtained during this 90-day period only. The data consist of arrays of latitude and longitude at 6-h intervals obtained by means of a procedure of objective interpolation (like kriging) described by Hansen and Poulain (1996).

Figure 1 ⊙= is a summary plot of the 19 free-drifting buoy tracks used for the analysis. The tracks present a rather confusing picture. As can be seen "by eye," the drifters were generally involved in some rotational, eddylike motions with a typical diameter of 100–200 km. It is worth noting that the drifter tracks cover two separate regions (see a dashed line in Fig. 1 ⊙=) connected by a short section near 35.5°N, 127°W, where all tracks nearly overlay. To treat this sort of inhomogeneity we performed the calculations in the whole area as well as in two separate regions.

3. Method and data processing

Suppose that we are able to observe a sufficiently large number of independent pairs of Lagrangian particles, provided that the particle separation covers a sufficiently wide range of length scales. In this case, we select all pairs with a given value of the separation, r (i.e., the distance between particles in a pair) and decompose particle velocity vectors $\mathbf{v}_1$ and $\mathbf{v}_2$ into longitudinal and transverse components, υ_{1L}, υ_{2L} and υ_{1N}, υ_{2N}, respectively (i.e., calculate projections of the velocity vectors on a separation vector $\mathbf{r} = \mathbf{r}_2 - \mathbf{r}_1$ of each pair and the respective right-orthogonal vector). Here $\mathbf{r}_1$ and $\mathbf{r}_2$ are the radius vectors of the particles in a pair; indices 1 and 2 refer to the first and second particle, respectively. Then, calculating the mean square of differences $\upsilon_{2L} - \upsilon_{1L}$ and $\upsilon_{2N} - \upsilon_{1N}$, we get estimates of longitudinal and transverse structure functions

$$D_{LL}(r) = \langle (\upsilon_{2L} - \upsilon_{1L})^2 \rangle_r,$$

$$D_{NN}(r) = \langle (\upsilon_{2N} - \upsilon_{1N})^2 \rangle_r, \qquad (1)$$

where $\langle \cdots \rangle_r$ denotes the ensemble averaging over pairs with a given value of the separation r. Of course, doing this, we suggest that the 2D velocity field is a stationary homogeneous isotropic random field.

Using the structure functions, we can calculate longitudinal and transverse autocorrelation functions

$$B_{LL}(r) = \overline{\upsilon'^2} - D_{LL}(r)/2,$$

$$B_{NN}(r) = \overline{\upsilon'^2} - D_{NN}(r)/2, \qquad (2)$$

where $\overline{\upsilon'^2} = (\langle \upsilon'^2_L \rangle + \langle \upsilon'^2_N \rangle)/2$; $\langle \upsilon'^2_L \rangle$ and $\langle \upsilon'^2_N \rangle$ are variances of the longitudinal and transverse velocity components, respectively; and $\langle \cdots \rangle$ is the ensemble averaging over all particle pairs in the area under consideration. Note that in the case of isotropy $\langle \upsilon'^2_L \rangle = \langle \upsilon'^2_N \rangle$ so that comparing empirical values of $\langle \upsilon'^2_L \rangle$ and $\langle \upsilon'^2_N \rangle$ we can judge how far from isotropy the velocity field is. Finally, the longitudinal and transverse one-dimensional two-sided spectra are calculated by taking the one-dimensional Fourlier transform of the autocorrelation functions $B_{LL}(r)$ and $B_{NN}(r)$

$$F_1(k_1) = 2 \int_0^\infty \cos(2\pi k_1 r) B_{LL}(r) \, dr,$$

$$F_2(k_1) = 2 \int_0^\infty \cos(2\pi k_1 r) B_{NN}(r) \, dr, \qquad (3)$$

where k_1 is the cyclic wavenumber.

Strictly speaking, in addition to stationarity, homogeneity and isotropy of the velocity field, the above approach assumes a homogeneous distribution of drifters in the area under consideration. In reality, estimates of the structure functions may be biased due to preferred positions of the Lagrangian particles [so-called array bias in the Davis (1991) terminology]. For example, being deployed simultaneously in a small area of about 20 km × 20 km, a cluster of 19 drifters that we use for

analysis was expanding with time due to turbulent diffusion. Therefore, estimating the mean values of longitudinal velocity and that of transverse velocity for the first and second particle separately and taking respective differences

$$\Delta v_L(r) = \langle v_{2L} \rangle_r - \langle v_{1L} \rangle_r,$$

$$\Delta v_N(r) = \langle v_{2N} \rangle_r - \langle v_{1N} \rangle_r \qquad (4)$$

we will usually get a positive value for $\Delta v_L(r)$ due to turbulent diffusion. It is also possible that we will get a nonzero value for Δv_N, which implies that the drifters being located in a limited area are involved in a large-scale cyclonic (anticyclonic) rotation provided that $\Delta v_N > 0$ ($\Delta v_N < 0$). Nonzero values of Δv_L and Δv_N should be considered as array biases because they are expected to vanish when drifters are homogeneously distributed everywhere in a homogeneous isotropic velocity field.

To eliminate (or at least reduce) the effect of array biases on estimates of the structure functions, we use modified formulas instead of (1):

$$D_{LL}(r) = \langle (v_{2L} - v_{1L} - \Delta v_L)^2 \rangle_r$$

$$D_{NN}(r) = \langle (v_{2N} - v_{1N} - \Delta v_N)^2 \rangle_r. \qquad (1')$$

Similarly, the longitudinal and transverse variances in (2) are estimated as

$$\langle v_L'^2 \rangle = \frac{1}{N} \sum_r \langle v_L'^2 \rangle_r n(r); \qquad \langle v_N'^2 \rangle = \frac{1}{N} \sum_r \langle v_N'^2 \rangle_r n(r);$$

$$N = \sum_r n(r), \qquad (5)$$

where

$$\langle v_L'^2 \rangle_r = 0.5(\langle v_{1L}^2 \rangle_r + \langle v_{2L}^2 \rangle_r - \langle v_{1L} \rangle_r^2 - \langle v_{2L} \rangle_r^2)$$

$$\langle v_N'^2 \rangle_r = 0.5(\langle v_{1N}^2 \rangle_r + \langle v_{2N}^2 \rangle_r - \langle v_{1N} \rangle_r^2 - \langle v_{2N} \rangle_r^2). \qquad (6)$$

Here $n(r)$ is the number of particle pairs with separation r, and N is the total number of pairs.

Using data of 19 drifters (Fig. 1 ⊙−), we produced 60 estimates of structure functions at $r = 10, 20, 30, \cdots, 600$ km, or at $r_i = 10i$ km, $i = 1, 2, \cdots, 60$, so that intervals of r to provide averaging were defined as $r_i - 5$ km $< r < r_i + 5$ km. Then, these estimates were smoothed by a plain three-point filter $\bar{D}_i = 0.5D_i + 0.25(D_{i-1} + D_{i+1})$ so that actually we obtain 30 independent estimates of the structure functions at space lags $20i$ km, $i = 1, 2, \cdots, 30$.

The data we analyze were taken from the California Current region in which the flow is far from homogeneity and stationarity. In principle, this may distort considerably results of the calculations. To address the distorting effect of inhomogeneity and nonstationarity we have carried out the calculations in two different regions, separated by a dashed line in Fig. 1 ⊙−, as well as in the whole area.

Estimates of $D_{LL}(r)$, $D_{NN}(r)$, $\Delta v_L(r)$, $\langle v'^2_L \rangle_r / \langle v'^2_N \rangle_r$, and $n(r)$ are presented in Fig. 2 ⊙−. In the whole area and the northern region, $D_{LL}(r)$ grows with r more or less monotonically, approaching respective value of $\overline{v'^2}$ (horizontal lines in Fig. 2 ⊙−) at $r \approx 400$ km: $D_{NN}(r)$ grows faster than $D_{LL}(r)$ at small lags so that it exceeds $\overline{v'^2}$ at $r \approx 100$ and then decreases slowly, approaching $\overline{v'^2}$ from above at $r \approx 400$ km. Such a behavior of structure functions is typical for turbulent flows (Tennekes and Lumley 1972; Monin and Yaglom 1975). At larger lags $r > 400$ km both $D_{LL}(r)$ and $D_{NN}(r)$ decrease with r, and we do not see any physical reason for it except for inhomogeneity of the velocity field at large scales and the lack of data. Note that the behavior of $\Delta v_L(r)$ and $\langle v'^2_L \rangle_r / \langle v'^2_N \rangle_r$ are quite expected and reasonable: $\Delta v_L(r) > 0$ (expansion of the drifter cluster due to turbulent diffusion), while estimates of $\langle v'^2_L \rangle_r / \langle v'^2_N \rangle_r$ in general are not far from unity so that the mean ratio $\langle v'^2_L \rangle / \langle v'^2_N \rangle$ is 1.15 in the whole area and 1.19 in the northern region.

In the southern region, the behavior of structure function at $r < 250$ km in general is similar to that of the whole area and the northern region at $r < 400$ km. However, at $r > 250$ km $D_{LL}(r)$ exhibits unexpected sudden growth, which is accompanied with sudden increase of $|\Delta v_L(r)|$ and, therefore, may be interpreted as a result of inhomoheneity of the flow. Note that in this case $\langle v'^2_L \rangle / \langle v'^2_N \rangle = 1.47$ so that the isotropy assumption is questionable here.

Because any dependable information about the behavior of structure functions at large space lags is not available, we will

take constant values for $D_{LL}(r)$ and $D_{NN}(r)$ at $r > 400$ km (the whole area and the northern region) and $r > 250$ km (the southern region). These asymptotic values are shown in Fig. 2 ⬤ by horizontal lines. Note that in the case of the southern region, the asymptotic value is just the mean value of both $D_{LL}(r)$ and $D_{NN}(r)$ in a range 190 km $< r <$ 250 km and does not coincide with calculated velocity variance (in contrast to the whole area and northern region cases).

Figure 3 ⬤ presents estimates of correlation functions $B_{LL}(r)$ and $B_{NN}(r)$ calculated using the structure functions taken from Fig. 2 ⬤. To make the analysis procedure more convincing we added to our data the longitudinal and transverse autocorrelations obtained by Poulain and Niiler (1989) using data of two clusters of drifters released in the California Current System in 1985 and 1986 approximately at 32° and 36°N, as well as those of two clusters of drifters deployed in the North Atlantic (Krauss et al. 1990). Despite the fact that estimates of $B_{LL}(r)$ and $B_{NN}(r)$ by Poulain and Niiler (1989) and Krauss et al. (1990) were obtained using an approach somewhat different from ours [following Middleton and Garrett (1986), the authors did not calculate the structure function to arrive at the Eilerian autocorrelation] the results are quite comparable.

To calculate power spectra, we added zeros to the autocorrelations shown in Fig. 3 ⬤ at large lags as far as $r = 600$ km (to increase resolution in wavenumbers) and then made "standard" Fourier transform with the Hanning lag weighting function (Bendat and Piersol 1971). The spectra are presented in Fig 5 ⬤.

4. Interpretation of empirical estimates of spatial correlations and spectra

a. General description

All empirical $B_{LL}(r)$ curves as well as $B_{NN}(r)$ curves have generally the same shape: Here $B_{LL}(r)$ decreases monotonically vanishing at large r; $B_{NN}(r)$ decreases faster than $B_{LL}(r)$ at small r, becomes negative at an intermediate range of r, and then approaches zero from below at large r. Such behavior of $B_{LL}(r)$ and $B_{NN}(r)$ curves is typical for turbulent flows (e.g., Tennekess and Lamley 1972) and can be explained using next the two expressions. First, in the case of isotropy, the correlation tensor $B_{jk}(\mathbf{r})$ has the form (Monin and Yaglom 1975)

$$B_{jk}(\mathbf{r}) = [B_{LL}(r) - B_{NN}(r)]\frac{r_j r_k}{r^2} + B_{NN}(r)\delta_{jk}, \qquad (7)$$

where $\delta_{jk} = 1$ at $j = k$ and $\delta_{jk} = 0$ at $j \neq k$. Second, in terms of the correlation tensor, the zero divergence condition has the form

$$\frac{\partial B_{jk}(\mathbf{r})}{\partial r_k} = \frac{\partial B_{jk}(\mathbf{r})}{\partial r_j} = 0, \qquad (8)$$

where repeated indices imply the summation. In view of (7), condition (8) can be rewritten as

$$B_{NN}(r) = B_{LL}(r) + \frac{r}{2}\frac{d}{dr}B_{LL}(r) \qquad (9)$$

in the 3D case (Monin and Yaglom 1975) and

$$B_{NN}(r) = B_{LL}(r) + r\frac{d}{dr}B_{LL}(r) \qquad (10)$$

in the 2D case (Middleton and Garrett 1986). Integrating (9) and (10) yields

$$\int_0^\infty rB_{NN}(r)\, dr = \int_0^\infty \frac{d}{dr}\left[\frac{r^2}{2}B_{LL}(r)\right] dr$$

$$= 0, \quad \text{3D case} \qquad (9')$$

$$\int_0^\infty B_{NN}(r)\, dr = \int_0^\infty \frac{d}{dr}[rB_{LL}(r)]\, dr$$

$$= 0, \quad \text{2D case.} \qquad (10')$$

Note that the 2D field of ocean currents, strictly speaking, is not a zero-divergence field because $u_x + \upsilon_y = -w_z \neq 0$. Therefore, using (10') to explain the shape of drifterborne spatial correlations and spectra, we should keep in mind that this is an approximation only.

In view of (9′) and (10′), the transverse autocorrelation has to be negative in some range of r, which is clearly seen in Fig. 3 ⊙. Moreover, expressions (9′) and (10′) together with the empirical $B_{LL}(r)$ in Fig. 3 ⊙ do explain the shape of $F_1(k_1)$ and $F_2(k_1)$ spectra. Indeed, if $B_{LL}(r)$ is positive at any r (this suggestion is approximately valid in all cases presented in Fig. 3 ⊙), the longitudinal spectrum $F_1(k_1)$ will have the maximum at the origin ($k_1 = 0$), which results directly from the definition (3) and is in accordance with empirical spectra in Fig. 4 ⊙. From (10′) and (3) we may conclude that $F_2 = 0$ at $k_1 = 0$ in 2D isotropic case so that $F_2(k_1)$ must have the maximum at some $k_1 > 0$, which is in good accordance with all empirical spectra in Fig. 4 ⊙. Note that in the 3D case we would get $F_2(0) = F_1(0)/2 > 0$, which results directly from (9′) and (3). Finally, since $F_1(k_1)$ and $F_2(k_1)$ are even functions with no discontinuity in their derivatives at $k_1 = 0$, $F_1(k_1)$ and $F_2(k_1)$ curve parabolically down and up, respectively, away from $k_1 = 0$.

Therefore, we may conclude that the shape of the empirical spatial correlations $B_{LL}(r)$ and $B_{NN}(r)$ and power spectra $F_1(k_1)$ and $F_2(k_1)$ corresponds well with the above theoretical predictions.

b. A stochastic model of drifterborn spatial correlations and spectra

In section 4a we explained the shape of empirical spatial spectra and correlations on the basis of isotropic turbulence theory. However, it does not help us to relate the obtained longitudinal and transverse spectra to some physical parameters. To do this, we develop a simple kinematic stochastic model of two-dimensional eddies.

To avoid confusion, it seems reasonable to discuss the difference between this consideration and the well-known spectral models of 2D turbulence by Kraichnan (1967) and Charney (1971). Suppose that some process (say, baroclinic instability) is responsible for generation of quasi-two-dimensional mesoscale eddies with typical length scale λ. Theories by Kraichnan (1967) and Charney (1971) are designed to describe special structure of the eddies in some equilibrium range of wavenumbers $k_1 \gg 1/\lambda$ (or even $k_1 \ll 1/\lambda$), which is established (if any) due to nonlinear interaction between eddies (so-called cascade process). In contrast, we are trying to describe the spectral structure of eddies only at length scales of their origin, that is, at $k_1 \sim 1/\lambda$, no matter whether any cascade process does exist.

Let us suppose that the xy plane is filled with randomly spaced two-dimensional axisymmetric eddies. The velocity field of each eddy is described by formulas

$$\left. \begin{array}{l} u_\varphi(r, t) = R\omega \exp(-t/T_*)f(r/R) \\ u_r(r, t) = 0 \end{array} \right\} \qquad r = [(x - x_0)^2 + (y - y_0)^2]^{1/2}, \qquad (11)$$

where u_r, u_φ are the radial and azimuthal velocity; ω is the angular velocity of eddy rotation; $t \geq 0$ is the "age" of the eddy (the time passed from its origin); T_* is the "lifetime" of the eddy, R is the radius of the eddy, x_0, y_0 are the coordinates of the eddy center, and $f(\zeta)$ is a function describing the shape of azimuthal velocity distribution in the eddy. To determine how the spectra depend on the shape of the velocity field in the eddy, we consider three functions for $f(\zeta)$:

$$
\begin{array}{lll}
1) & & \zeta \exp(-\zeta^2/2) & (12) \\
& & \\
2) & f(\zeta) = \begin{cases} \zeta[1 + \cos(a\zeta)]/2, & a\zeta \leq \pi \\ 0, & a\zeta > \pi \end{cases} & (13) \\
& & \\
3) & & \zeta \exp(-\zeta), & (14)
\end{array}
$$

where $a = 1.306\ 54$ is a constant whose value is chosen to ensure the maximum of $f(\zeta)$ at $\zeta = 1$. Functions (12)–(14) are shown in Fig. 5 ⊙.

Let us define our stochastic process as a process in which N_{birth} eddies given by (11)–(14) are born per unit time in a square domain $L \times L$, $L \gg R$, provided that each eddy birth is an independent event and the probability of eddy birth is uniform by the domain. The velocity field in the domain is determined as a linear superposition of velocities of each eddy.

The velocity field in the domain interior, except its marginal areas with typical width several times greater than R, may be considered as a random, stationary, homogeneous, isotropic 2D field. Our goal is to obtain spectra $F_1(k_1)$ and $F_2(k_1)$ for this model field.

In general, the model spectra $F_1(k_1)$ and $F_2(k_1)$ will depend on four parameters: ω, N_{birth}/L^2 (the number of eddies born per unit time and area), T_*, and R, as well as the wavenumber k_1. Because only two dimensions are involved (time and length), we can construct three dimensionless variables. However, we may suppose the existence of a self-similarity that reduces all variety of spectra $F_1(k_1)$ and $F_2(k_1)$ to some functions of one variable. Of course, the shape of self-similar spectra will depend on the shape of the eddy given by formulas (12) or (13) or (14).

The total kinetic energy (E_{eddy}) of each eddy may be estimated as

$$E_{eddy} \approx D(\omega R)^2 R^2, \quad (15)$$

where D is the 2D density (mass per unit area).

The mean number of eddies per unit area is

$$\rho_{eddy} \approx N_{birth} T* / L^2. \quad (16)$$

The total energy of eddies per unit area, E_{total}, is

$$E_{total} = E_{eddy} \rho_{eddy} \approx D \frac{N_{birth} T*}{L^2} \omega^2 R^4. \quad (17)$$

Therefore, the variance of the velocity field $\overline{v'^2}$ is estimated as

$$\overline{v'^2} \approx \frac{E_{total}}{D} \approx \frac{N_{birth} T*}{L^2} \omega^2 R^4. \quad (18)$$

If we suppose that spectra $F_1(k_1)$ and $F_2(k_1)$ are determined by $\overline{v'^2}$, R, and k_1, and apply dimensional analysis, we obtain self-similar forms

$$F_1(k_1) = \frac{N_{birth} T*}{L^2} \omega^2 R^5 f_1(k_1 R)$$

$$F_2(k_1) = \frac{N_{birth} T*}{L^2} \omega^2 R^5 f_2(k_1 R), \quad (19)$$

where $f_1(\xi_1), f_2(\xi_1)$ are some functions of a dimensionless wavenumber $\xi_1 = k_1 R$.

We realize that (19) is a hypothesis only. To prove it, we address numerical simulations of the random field defined above.

We choose a domain 4000 km × 4000 km and, using a random number generator, produce rows of coordinates of eddy center $x_0(i)$ and $y_0(i)$, $i = 1, 2, 3, \cdots$, randomly spaced in the domain with uniform probability. Prescribing some values of parameters ω, $T*$, R, and identifying time in (11) with numbering i of the succession $[x_0(i), y_0(i)]$, we compute the velocity field as the superposition of velocities of each eddy (11). The truncation of the succession is determined by a condition

$$\exp(-i/T*) \leqslant A_{small}, \quad (20)$$

where $A_{small} \ll 1$ is the truncation constant. In our numerical experiments, we take $A_{small} = 1 \times 10^{-3}$ and vary the governing parameters in the following ranges: $10 \text{ km} \leqslant R \leqslant 100 \text{ km}$, $0.4 \times 10^{-5} \text{ s}^{-1} \leqslant \omega \leqslant 3 \times 10^{-5} \text{ s}^{-1}$, $800 \leqslant T* \leqslant 24\,000$. The spectra $F_1(k_1)$ and $F_2(k_1)$ were calculated as the Fourier transform of the correlation function, that is, using exactly the same approach we had used to calculate the empirical drifterborne spectra.

When normalized by (19), all model spectra computed at different values of parameters ω, R, $T*$ and the same eddy shape merge into one. Therefore, the self-similarity suggested above is validated. Figure 6 presents self-similar model spatial spectra and correlations for three different eddy shapes (12)–(14).

In general, all three pairs of self-similar spectra $F_1(k_1)$ and $F_2(k_1)$ and correlations $B_{LL}(r)$ and $B_{NN}(r)$ in Fig. 6 resemble one another and reproduce well the shape of the empirical drifterborne spatial spectra and correlations presented in Figs. 3 and 4 . Since the model is based on simple and physically clear assumptions, it may be considered as a physical interpretation of drifterborne spatial spectra and correlations. We have not seen in the literature a more simple and clear interpretation of longitudinal and transverse correlations and spectra.

Closer inspection of Fig. 6 reveals that statistical population of eddies with different shape produces spatial spectra and correlations of different shape. For example, the exponential eddy (14) with a relatively long "tail" of slowly decreasing velocity at large distances produces long tails of $F_2(k_1)$ and $B_{NN}(r)$ at large k_1 and r, respectively. To determine which eddy shape, (12), (13), or (14), offers a better description of empirical spatial spectra, we present all the spectra, both empirical and model ones, in a normalized form

$$F_1 \tilde{k}_1 / \overline{v'^2} = f_1(k_1/\tilde{k}_1); \qquad F_2 \tilde{k}_1 / \overline{v'^2} = f_2(k_1/\tilde{k}_1), \quad (21)$$

where $\tilde{k}_1$ is the wavenumber at which $F_2(k_1)$ is the maximum.

The normalized spectra are shown in Fig. 7 ⊙━. Despite considerable scatter of the empirical spectral estimates, the model with exponential eddy shape appears to fit the empirical spectra much better than those of Gaussian and cosine eddy shapes. Physically, this implies that mesoscale ocean eddies consist of a relatively small core with solid-body rotation so that the transverse velocity is maximum at the outer edge of the core and there is much wider peripheral "ring" where the velocity is about constant (inner periphery) and then slowly decreases with distance outward from the eddy center (outer periphery).

In order to test this issue quantitatively, we calculate a mean square deviation (MSD) of the empirical spectral estimates in Fig. 7 ⊙━ from respective model curves. It is found that the MSD produced by the model with exponential eddy shape is 1.8 and 2.1 times smaller than that of the Gaussian and cosine eddy shapes, respectively. We also calculate MSD using the best-fit curve of a sixth power polynomial to the normalized empirical spectra instead of the empirical spectral estimates themselves (dotted lines in Fig. 7 ⊙━). The result is found to be even more convincing: MSD for the exponential eddy model (14) is 6.3 and 8.7 times smaller than that of models (12) and (13), respectively.

c. Length scales derived from the spatial spectra

Since all empirical spectra $F_2(k_1)$ display clearly the maximum at some $k_1 = \tilde{k}_1$, it seems reasonable to estimate the respective spectral length scale $\tilde{\Lambda} = 1/\tilde{k}_1$ and, in the wake of Krauss et al. (1990), compare it with the internal Rossby radius R_i. In addition to $\tilde{\Lambda}$ and R_i, we will compare respective radii of model eddies (12)–(14) which provide the best fit of the empirical spectra (i.e., when the model transverse spectrum is the maximum at the same wavenumber $k_1 = \tilde{k}_1$): $R_1 = 0.162 \tilde{\Lambda}$, $R_2 = 0.199\tilde{\Lambda}$, and $R_3 = 0.0859\tilde{\Lambda}$ (the Gaussian, cosine, and exponential eddy shapes, respectively).

The wavenumber of spectral maximum $\tilde{k}_1$ was estimated by the parabolic interpolation of the empirical spectrum $F_2(k_1)$ in the vicinity of its maximum. For R_i, we took estimates of the internal Rossby radius calculated by Emery et al. (1984) by solving respective eigenvalue problems with annual mean vertical profiles of Brunt–Väisälä frequency by 5° squares for the North Pacific and the North Atlantic.

Estimates of $\tilde{\Lambda}$, R_1, R_2, R_3, and R_i for six pairs of empirical spectra $F_1(k_1)$ and $F_2(k_1)$ shown in Fig. 4 ⊙━ are given in Table 1 ⊙━. One cannot miss surprisingly good coincidence of the estimates of the best-fit radius of exponential eddy R_3 and the internal Rossby radius R_i for all clusters of drifters in the California Current System (cases 1–4) and the North Atlantic Current (case 5). We suppose that this coincidence is not casual. In the Newfoundland Basin (case 6), correspondence between R_3 and R_i is worse (36 km vs 20.6 km).

5. Conclusions

We have suggested a particle pair approach to estimate spatial spectra of mesoscale horizontal turbulence in the ocean using data of satellite-tracked drifters. The approach was applied to the data of 19 drifters deployed simultaneously in the California Current System in 1993. We also calculate power spectra from longitudinal and transverse correlations obtained by Poulain and Niiler (1989) (a cluster of drifters deployed in the California Current System in 1985/86) and Krauss et al. (1990) (two clusters of drifters deployed in the North Atlantic Current and the Newfoundland Basin, respectively).

In all cases, spectra $F_1(k_1)$ as well as spectra $F_2(k_1)$ occurred to have the same shape: being the maximum at the origin ($k_1 = 0$), $F_1(k_1)$ decreases monotonically vanishing at large k_1, while $F_2(k_1)$ is the maximum at some $k_1 = \tilde{k}_1 > 0$ and vanishes at $k_1 \rightarrow \infty$ and $k_1 \rightarrow 0$. Such a behavior of empirical estimates of $F_1(k_1)$ and $F_2(k_1)$ is in accordance with theoretical predictions for 2D isotropic nondivergent turbulent flow.

To determine the shape of $F_1(k_1)$ and $F_2(k_1)$ in more detail, we have developed stochastic models consisting of a population of randomly spaced, two-dimensional axisymmetric eddies of a given shape. Numerical experiments with different eddy shapes (the Gaussian, cosine, and exponential shapes of the transverse velocity were applied) showed that the model spectra obey a self-similarity, that is, for a given eddy shape they depend on the variance of stochastic process and a length scale (radius) of the eddy only. Comparing self-similar model spectra with the empirical ones, we found that a model with exponential eddy shape fits drifterborne $F_1(k_1)$ and $F_2(k_1)$ much better than the other models. It may be physically interpreted as if mesoscale ocean eddies consist of a relatively small core with solid-body rotation and a much wider peripheral ring where the velocity is about constant in the inner part of the ring and slowly decreasing with the distance outward from the eddy center in the outer part of the ring.

We have found that the best agreement between the drifterborne and model spectra is achieved when the radius of an exponentially shaped model eddy is taken equal to the internal Rossby radius.

REFERENCES

Bendat, J. S., and A. G. Piersol, 1971: *Random Data: Analysis and Measurement Procedures.* Wiley-Interscience, 407 pp..

Charney, J. G., 1971: Geostrophic turbulence. *J. Atmos. Sci.,* **28,** 1087–1095.. Find this article online

Davis, R. E., 1985: Drifter observations of coastal surface currents during CODE: The statistical and dynamical views. *J. Geophys. Res.,* **90,** 4756–4772..

—— ,1987: Modeling eddy transport of passive tracers. *J. Mar. Res.,* **45,** 635–666..

—— ,1991: Observing the general circulation with floats. *Deep-Sea Res.,* **38,** S531–S571..

Emery, W. J., W. G. Lee, and L. Magaard, 1984: Geographic and seasonal distributions of Brunt–Väisälä frequency and Rossby radii in the North Pacific and North Atlantic. *J. Phys. Oceanogr.,* **14,** 294–317.. Find this article online

Figueroa, H. A., and D. B. Olson, 1989: Lagrangian statistics in the South Atlantic as derived from SOS and FGGE drifters. *J. Mar. Res.,* **47,** 525–546..

Grifa A., K. Owens, L. Piterbarg, and B. Rosovskii, 1995: Estimates of turbulence parameters from Lagrangian data using a stochastic particle model. *J. Mar. Res.,* **53,** 371–401..

Hansen, D. V., and P.-M. Poulain, 1996: Quality control and interpolation of WOCE/TOGA drifter data. *J. Atmos. Oceanic Technol.,* **13,** 900–909..

Krauss, W., and C. W. Boning, 1987: Lagrangian properties of eddy fields in the northern North Atlantic as deduced from satellite-tracked buoys. *J. Mar. Res.,* **45,** 259–291..

—— ,R. Döscher, A. Lehmann, and T. Viehoff, 1990: On eddy scales in the northern North Atlantic Ocean as a function of latitude. *J Geophys. Res.,* **95,** 18 049–18 057..

Kraichnan, R. H., 1967: Inertial ranges in two-dimensional turbulence. *Phys. Fluids,* **10,** 1417–1423..

Middleton, J. F., and C. Garrett, 1986: A kinematic analysis of polarized eddy fields using drifter data. *J. Geophys. Res.,* **91,** 5094–5102..

Monin, A. S., and A. M. Yaglom, 1975: *Statistical Fluid Mechanics:Mechanics of Turbulence.* Vol. 2. The MIT Press, 874 pp..

Poulain, P.-M., and P. P. Niiler, 1989: Statistical analysis of the surface circulation in the California Current System using satellite-tracked drifters. *J. Phys. Oceanogr.,* **19,** 1588–1603.. Find this article online

Rossby, H. T., S. C. Riser, and A. J. Mariano, 1983: The western North Atlantic—A Lagrangian viewpoint. *Eddies in Marine Science,* A. R. Robinson, Ed., Springer-Verlag, 66–91..

Swenson, M. S., and P. P. Niiler, 1996: Statistical analysis of the surface circulation of the California Current. *J. Geophys. Res.,* **101,** 22 631–22 645..

Tennekes, H., and J. L. Lumley, 1972: *A First Course in Turbulence.* The MIT Press, 300 pp..

APPENDIX

6. Confidence Intervals

Following Middleton and Garrett (1986), confidence intervals for normalized structure functions and autocorrelation functions can be calculated using the Fisher distribution with n_1 and n_2 degrees of freedom (Bendat and Piersol 1971),

where n_1 is the degrees of freedom for $D_{LL}(r)$ and $D_{NN}(r)$ estimates and n_2 is that of $\overline{\upsilon'^2}$. In our case, $n_1(n_2)$ is the number of independent estimates of particle pair velocity (particle velocity) included in the averaging. To treat the independence, two issues were taken into account. First, the particle pair velocity (particle velocity) estimate is considered as independent if it is lagged by an independence time $\tau_{ind} = 2T_L$, where T_L is the Lagrangian integral timescale. Estimating T_L by the first zero crossing of the Lagrangian autocorrelation function, we obtain $\tau_{ind} = 10$ days. Second, if the statistics is based on N_d drifters, so that $N_d(N_d - 1)/2$ pairs are available, no more than $2N_d$ pairs are independent because this is just the number of coordinates for N_d drifters. Therefore, if an estimate of the structure function at a given value of the space lag r is based on $n(r)$ estimates of the pair velocity, the degrees of freedom are

$$n_1 = n(r)f(N_d)\Delta t/\tau_{ind}, \quad (A1)$$

where $f(N_d) = \min(1, 4/(N_d - 1)$ and Δt is the sampling time (6 h). Similarly, the degrees of freedom for $\overline{v'^2}$ are

$$n_2 = 4Nf(N_d)\,\Delta t/\tau_{ind},\quad\text{(A2)}$$

where the factor 4 is because every particle pair yields four estimates of velocity components.

In the whole area and the northern region in Fig. 1 ⊙▬, $N_d = 19$ so that $f(N_d)\Delta t/\tau_{ind} = 1/180$, while in the southern region $N_d = 12$ so that $f(N_d)\Delta t/\tau_{ind} = 1/110$. Typical value of $n(r)$ at $r < 250$ km is 2400, 1500, and 700 in the whole area, and the northern and southern regions, respectively, so that respective estimates of n_1 are 13.3, 8.3, and 6.4. Because in all cases $n_2 > 300$ we may take $n_2 = \infty$. Ultimately, the 95% confidence intervals for the structure function are $(0.46–1.71)D(r)$, $(0.35–1.94)D(r)$, and $(0.29–2.08)D(r)$ at $r < 250$ km in the three cases, respectively. The confidence intervals grow fast at $r > 250$ due to the decrease of $n(r)$.

Tables

Table 1. The comparison between the empirical spectral length scale $\bar{\lambda}$; the best-fit radii of Gaussian, cosine, and exponential model eddies (R_1, R_2, R_3, respectively) and the internal Rossby radius R_i. The cases are numbered in accordance with Fig. 3.

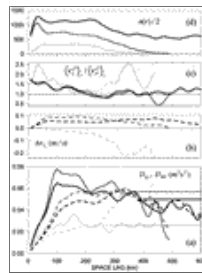|	Case					
	1	2	3	4	5	6
$\bar{\lambda}$ (km)	355	327	360	341	222	413
R_1 (km)	57	53	58	55	36	67
R_2 (km)	71	65	72	68	44	82
R_3 (km)	30	28	31	29	19	36
R_i (km)	26.7	26.7	27.8	27.8	16.6	20.6

Click on thumbnail for full-sized image.

Figures
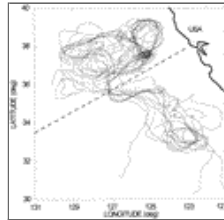
Click on thumbnail for full-sized image.

Fig. 1. Summary plot of 19 free-drifting buoy tracks used in the analysis.

Click on thumbnail for full-sized image.

Fig. 2. (a) Empirical structure functions (D_{LL}: dashed, D_{NN}: solid), (b) mean difference of longitudinal pair velocities Δv_L, (c) ratio of longitudinal to transverse velocity variances $\langle v'^2{}_L\rangle_r/\langle v'^2{}_N\rangle_r$, and (d) the number of particle pairs n vs the space lag r. Bold, regular, and thin lines refer to the whole area, northern region, and southern region, respectively (see Fig. 1 ⊙▬).
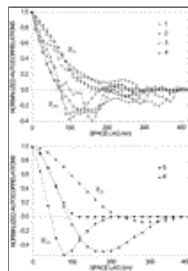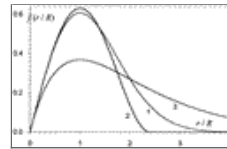

Click on thumbnail for full-sized image.

Fig. 3. Normalized autocorrelation functions $B_{LL}(r)$ (dotted) and $B_{NN}(r)$ (solid): 1, 2, 3—the whole area, northern region, and southern region, respectively (see Fig. 1 ⬤▬); 4—a cluster of drifters deployed in the California Current System at 32° and 34°N [the curves were taken from (Poulain and Niiler 1989)]; 5 and 6—clusters of drifters in the North Atlantic Current and the Newfoundland Basin with the mean position 49.2°N, 42.9°W and 43.8°N, 43.4°W, respectively [the curves were taken from (Krauss et al. 1990)].
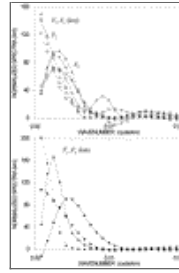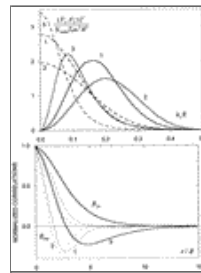

Click on thumbnail for full-sized image.

Fig. 4. Normalized longitudinal (F_1) and transverse (F_2) power spectra. For explanation, see Fig. 3 ⬤▬.
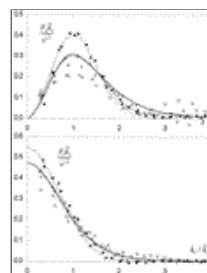

Click on thumbnail for full-sized image.

Fig. 5. The transverse velocity distribution in a model eddy given by formulas (12)–(14) indicated by isoplethes labeled 1, 2, and 3.

Click on thumbnail for full-sized image.

Fig. 6. Self-similar model spectra F_1 (dashed) and F_2 (solid) and correlations B_{LL} and B_{NN}. Numbered isoplethes (1, 2, 3) inside the panels refer to the eddy shape formulas (12), (13), (14), respectively.

Click on thumbnail for full-sized image.

Fig. 7. The comparison of the normalized empirical spectra and model spectra. Regular solid, thin solid, and thin dashed lines depict the model spectra with exponential, Gaussian, and cosine eddy shape, respectively. Dotted line is the best-fit curve of empirical spectra by a sixth power polynomial. The empirical spectra legend is given in Fig. 3 ⬤▬.

Corresponding author address: Dr. Im Sang Oh, Dept. of Oceanography, College of Natural Sciences, Seoul National University, Seoul 151-742, Korea.

E-mail: ois@storm.snu.ac.kr